High-pressure phase transformations, pressure-induced amorphization, and polyamorphic transition of the clathrate $Rb_{6.15}Si_{46}$

D. Machon,[1] P. Toulemonde,[1,2] P. F. McMillan,[3] M. Amboage,[4,5] A. Muñoz,[6] P. Rodríguez-Hernández,[6] and A. San Miguel[1]
[1]*LPMCN, Université Lyon-I, Bâtiment Léon Brillouin, 43 Boulevard du 11 Novembre 1918, F-69622 Villeurbanne Cedex, France*
[2]*Institut Néel, CNRS and Université Joseph Fourier, 25 Avenue des Martyrs, BP 166, F-38042 Grenoble Cedex 9, France*
[3]*Department of Chemistry and Materials Chemistry Centre, Christopher Ingold Laboratories, University College London, 20 Gordon Street, London WC1H 0AJ, United Kingdom*
[4]*European Synchrotron Radiation Facility, BP 220, F-38043 Grenoble Cedex 9, France*
[5]*Diamond Light Source, Harwell Science and Innovation Campus, Didcot, Oxfordshire OX11 0DE, United Kingdom*[*]
[6]*Departamento de Física Fundamental II, MALTA Consolider Team, Universidad de La Laguna, La Laguna, 38205 Tenerife, Spain*
(Received 17 November 2008; revised manuscript received 3 March 2009; published 4 May 2009)

The type-I clathrate $Rb_{6.15}Si_{46}$ with partly empty cage sites has been studied up to 36 GPa using Raman spectroscopy, synchrotron x-ray diffraction in diamond-anvil cells, and *ab initio* total-energy and lattice-dynamics calculations. A first phase transition is observed at 13 ± 1 GPa and a "volume collapse" transition within the clathrate structure is then observed at 24 ± 1 GPa. Pressure-induced amorphization into a high-density amorphous (HDA) state occurs above $P=33\pm1$ GPa. The HDA form transforms into a low-density amorphous polymorph during decompression. During the compression study using angle dispersive synchrotron x-ray diffraction techniques we measured bulk modulus parameters for rocksalt-structured TaO, included adventitiously in the clathrate sample [$K_0=293(3)$ GPa and $K_0'=5.4(3)$].

DOI: 10.1103/PhysRevB.79.184101 PACS number(s): 61.50.Ks, 64.60.My

I. INTRODUCTION

Since the first syntheses of alkali-doped Si and Ge "semiconductor clathrate" phases by the metastable thermal decomposition of Zintl compounds such as NaSi or NaGe (Refs. 1–3) or by direct reaction between the elements,[4] there has been increasing interest in this unusual family of solid-state materials.[5,6] Analogous clathrate structures are now known to occur with group 13–15 elements, halogens, chalcogenides, transition-metal atoms substituting for Si or Ge on framework sites, and various alkali or alkaline-earth atoms, halogens, chalcogenides, transition metals, and lanthanides occupying "guest" sites.[5–7] The semiconductor clathrates correspond to open framework structures formed by assemblage of T_{20}, T_{24}, or T_{28} polyhedral cages, where T=Si, Ge etc. atoms are in slightly distorted tetrahedral coordination with sp^3 bonding. The cages are fully or partly filled with guest atoms. Clathrate materials have received considerable attention because of their unusual and potentially useful electronic,[8] optical,[9] mechanical,[10] and thermoelectric[11] properties or as electron emitters[12] between others. Depending upon the degree of guest atom filling vs framework site occupancy, they exhibit electrical behavior ranging from semiconducting to metallic. Between others, clathrates in the systems $(Na_{1-x}Ba_x)_8Si_{46}$ and $(Ba_{1-x}Sr_x)_8Si_{46}$ are superconducting with T_c between 4 and 8 K.[13–15] The relationship between the electronic and vibrational properties of the framework vs guest atom sublattices is of particular interest giving rise to unique thermoelectric behavior.

We will adopt here the basic clathrate structure description based on three clathrate types which map on to structures formed by the H_2O-based clathrate hydrates.[16] More complete classifications have been also proposed to describe symmetry variations in ternary group-14 clathrates.[17] The type-I clathrate (space group $Pm\bar{3}n$) contains two Si_{20} and six Si_{24} polyhedral cages and it provides a total of eight (two small and six large) occupancy sites for guest atoms. That gives rise to compositions such as Na_8Si_{46} if all guest sites are filled or Rb_6Si_{46} if only the larger sites are occupied. These compounds are metallic because of the contribution from the alkali atom electrons to the conduction band.[18]

There have been many studies of high-pressure transformations among the stable and metastable polymorphs of elemental Si.[19] The diamond-structured polymorph of silicon transforms into the metallic β-Sn structured polymorph with the atoms in distorted octahedral coordination at 10.5 GPa,[20] followed by further transitions into dense metallic phases with the atoms in higher coordination at higher pressures.[21] A guest-free variety of the type-II clathrate Si_{136} has been prepared that constitutes a low-density allotrope of the element and that is metastable relative to the diamond structure at ambient pressure.[5,9,22] Based on the projected intersection of free-energy (G) curves, it was initially predicted that Si_{136} would transform into the β-Sn structure at a lowered pressure ($P\sim3-4$ GPa) compared to the diamond phase.[9] However, that result was not observed experimentally probably due to kinetic effects associated with Si-Si bond breaking and a direct transition to the β-Sn polymorph was observed at $P\sim8-10$ GPa using energy-dispersive synchrotron x-ray diffraction in a diamond-anvil cell.[23,24] A recent study using Raman spectroscopy has found that the situation is more complex and that at least one intermediate metastable phase is formed during the compression and collapse of the clathrate structure.[25]

Several studies have addressed the high-pressure behavior of clathrates with filled guest cages. Na_8Si_{46} apparently undergoes pressure-induced decomposition above $P=14$ GPa, where characteristic peaks of the metallic hexagonal structure of Si begin to appear in the x-ray diffraction pattern.[5,26] However, type-I clathrates with larger guest atoms

 ©2009 The American Physical Society

[K_8Si_{46},[27,28] Ba_8Si_{46},[29,30] and $I_8Si_{44}I_2$ (Refs. 5 and 31)] exhibit an unusual "volume collapse" transition in this pressure range while apparently retaining the same cubic clathrate crystal structure, followed by pressure-induced amorphization at higher pressure. That behavior and its dependence on the cage site occupancy are not well understood.

The clathrate compound $Rb_{6.15}Si_{46}$ is a particularly interesting case for study because the six Si_{24} cages are filled with the large Rb guest atoms (occupancy=0.952), but the occupancy of the smaller Si_{20} cages is substantially smaller than unity (occupancy=0.218).[9] It therefore constitutes a useful case to examine the different roles played by filling the two types of nanocages in determining the stability, mechanical properties, and pressure behavior of type-I clathrates. Here we use a combination of experimental (synchrotron angle-dispersive x-ray diffraction and Raman scattering) and *ab initio* calculation approaches to study the high-pressure behavior of the type-I clathrate $Rb_{6.15}Si_{46}$.

II. EXPERIMENTAL AND COMPUTATIONAL METHODS

The synthesis and characterization of $Rb_{6.15}Si_{46}$ were described previously and here we used samples obtained from that study.[9] The $Rb_{6.15}Si_{46}$ was synthesized from mixtures of elemental Rb and Si at 666 °C in a Ta capsule and sealed inside a steel bomb for 24 h. Excess alkali was removed from the silicide by evaporation at 250 °C under a vacuum of $\sim 10^{-5}$ Torr. The silicon clathrate sample was then obtained by evaporating the alkali atoms between 425 and 475 °C at a pressure of $\sim 10^{-6}$ Torr. Prior to carrying out high-pressure experiments, the sample was stored in a glove box (<10 ppm O_2/H_2O) at room temperature. Aliquots were removed from the sample for loading into diamond-anvil cells or to be carried to the synchrotron.

High-pressure *in situ* synchrotron x-ray diffraction experiments were carried out using a He gas membrane-driven diamond-anvil cell with diamonds having a culet size of 350 μm. Samples were loaded using nitrogen as a pressure-transmitting medium and the pressures were determined using the ruby fluorescence method.[32] Pressure was increased by steps of 1–2 GPa and the system was left to equilibrate for 15–30 min at each pressure.

Synchrotron radiation measurements were performed at the European Synchrotron Radiation Facility (ID9A) via angle-dispersive diffraction techniques using monochromatic radiation (λ=0.412 475 Å). Diffraction patterns were collected using image plate detection. The sample-to-detector distance and the image plate orientation angles were calibrated using a crystalline Si standard. The two-dimensional diffraction images were analyzed using the FIT2D software, yielding one-dimensional intensity vs diffraction angle 2θ patterns.[33]

High-pressure Raman-scattering experiments were carried out using a cylindrical diamond-anvil cell with low-fluorescence diamonds having a culet size of 200 μm. Pure polycrystalline $Rb_{6.15}Si_{46}$ was loaded into a 90 μm hole drilled in a Re gasket. The pressure-transmitting medium argon was cryogenically loaded as a fluid into the cell and used as a nearly hydrostatic medium during pressurization experiments. Several ruby chips were distributed throughout the sample chamber and the pressures were determined using the ruby fluorescence method.[32] A nonhydrostatic pressurization experiment was also carried out without any pressure-transmitting medium using the same experimental configuration.

Raman spectra were obtained using a home-built high-throughput optical system based on Kaiser optical notch filters and an Acton 300i spectrograph with sensitive charge coupled device (CCD) detection.[34] Spectra were excited using 514.5 nm radiation from an air-cooled Ar^+ laser. The beam was focused on to the sample using a Mitutoyo 50× objective with beam diameter $\sim$2 μm at the sample. The backscattered light was collected using the same lens.

Total energy and lattice dynamics calculations were carried out within the framework of density-functional theory (DFT) (Ref. 35) and the pseudopotential method using the Vienna *ab initio* simulation package (VASP) of which a detailed description of the methodology can be found in Ref. 36 and references therein. The exchange and correlation energies were initially formulated within the generalized gradient approximation (GGA) according to the Perdew-Burke-Ernzerhof[37] (PBE) prescription. The projector-augmented wave (PAW) scheme[38] was adopted and the semicore 4*s* electrons of Rb were dealt with explicitly in the calculations. The set of plane waves used extended up to a kinetic-energy cutoff of 350 eV. This cutoff was required to treat the atoms within the PAW scheme to ensure highly converged results. The Monkhorst-Pack[39] grid used for Brillouin-zone integrations ensured highly converged results (to about 1 meV per formula unit). We tested different meshes for the Rb_xSi_{46} analyzed structures. At each selected volume, the structures were fully relaxed to their equilibrium configuration through the calculation of the forces on atoms and the stress tensor (see Ref. 40). In the relaxed equilibrium configuration, the forces are less than 0.002 eV/Å and the deviation of the stress tensor from a diagonal hydrostatic form is less than 1 kbar (0.1 GPa). The highly converged results for the forces are required for the calculation of the dynamical matrix using the direct force-constant approach (or supercell method).[41] The construction of the dynamical matrix at the Γ point is particularly simple and involves separate calculations of the forces in which a fixed displacement from the equilibrium configuration of the atoms within the *primitive* unit cell is considered. Symmetry aids in the computations by reducing the number of such independent distortions and the amount of computational effort required. Diagonalization of the dynamical matrix provides both the frequencies of the normal modes and their polarization vectors. It allows us to identify the irreducible representation and the character of the phonon modes at the zone center.

III. RESULTS

A. X-ray diffraction

The x-ray diffraction pattern of the $Rb_{6.15}Si_{46}$ clathrate compound at ambient pressure is shown in Fig. 1. The main peaks can be assigned and indexed unambiguously as the clathrate type-I structure (space group: $Pm\bar{3}n$, No. 223). Us-

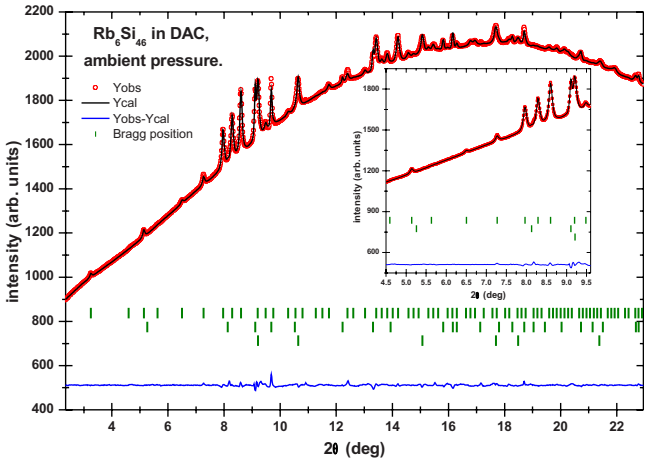

FIG. 1. (Color online) X-ray diffraction pattern including Rietveld refinement of the sample at room pressure in the diamond-anvil cell. Three phases are present: the type-I clathrate $Rb_{6.15}Si_{46}$ ($Pm\bar{3}n$), the ε phase of TaN ($P6\bar{2}m$), and TaO with rocksalt structure ($Fm\bar{3}m$).

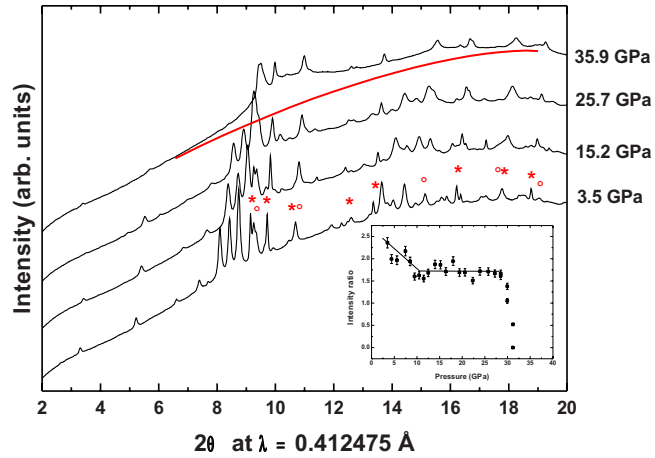

FIG. 2. (Color online) Selected x-ray diffraction patterns with increasing pressure. The peaks due to the ε-TaN phase and TaO are identified with asterisks and open circles, respectively. At pressure higher than 33 GPa the diffraction peaks from the clathrate $Rb_{6.15}Si_{46}$ disappear and are replaced by a broad amorphous signal indicating the occurrence of pressure-induced amorphization. The additional peaks are due to crystalline TaN and TaO. An estimated background line is drawn to show the likely amorphous contribution to the x-ray scattering at high pressure. Inset: intensity ratio between the (320) clathrate peak and the (200) TaO peak used as a standard. A small decrease of this ratio is observed between ambient pressure and 10 GPa followed by a sudden decrease of the $Rb_{6.15}Si_{46}$ peak intensity with a complete disappearance by 33 GPa that indicates amorphization of the clathrate structure.

ing Rietveld refinement, the cell parameter was 10.286(1) Å and the occupancy of the Si_{20} cages by Rb atoms was found to be 24%, in agreement with the previous determination.[9] However, we also observed a series of additional peaks in our diffraction pattern that were due to small amounts of (a) ε-TaN [space group: $P6$-$2m$, No. 189 with cell parameters a=5.1938(2) Å and c=2.9101(2) Å (Ref. 42)] and (b) TaO with the rocksalt structure [space group: Fm-$3m$, No. 225 with cell parameter a=4.4484(2) Å]. These impurity phases were introduced adventitiously during grinding the samples for synchrotron diffraction experiments in the diamond-anvil cell: the agate mortar had previously been used to grind samples of the ultrahard material ε-TaN: some grains remained embedded in the mortar and partly oxidized in air to give TaO; both phases were then transferred into our clathrate sample. From Rietveld analysis we estimate the ε-TaN and TaO concentrations in mass as 5.8(2)% and 8.4(2)%, respectively. The presence of these phases in our sample did not affect the interpretation of the synchrotron x-ray results on the $Rb_{6.15}Si_{46}$ clathrate sample: in fact, they provided a useful internal standard for the analysis of linewidths and relative intensities of clathrate features in our high-pressure x-ray diffraction measurements. In addition, our data allowed us to obtain a value for the compressibility of TaO.

In Fig. 2 we show selected diffraction patterns as a function of pressure. The TaN and TaO peaks are marked. The unit-cell parameters for all three phases were obtained at each pressure by LeBail refinements using the FULLPROF software,[43] allowing us to determine relative volume V/V_0 values. A plot of V/V_0 as a function of pressure for $Rb_{6.15}Si_{46}$ is shown in Fig. 3 using 32 peaks for $Rb_{6.15}Si_{46}$ to carry out the global LeBail refinement. A change in slope is clearly observed at 24 ± 1 GPa marking the presence of a "volume collapse" transition as previously observed for K-, Ba-, and I-containing clathrates.[5,27–31] As noted for the other clathrates, there are no obvious changes in the number or relative intensities of peaks in the x-ray diffraction pattern and none of the peaks exhibit any splitting, so it is proposed that the transition is "homothetic" or isostructural. At 29 ± 1 GPa, an abrupt decrease in intensity of the $Rb_{6.15}Si_{46}$ Bragg peaks is observed, relative to the TaO features that provide a useful internal intensity standard (Fig. 2 inset). By 33 ± 1 GPa, the clathrate peaks have completely disappeared and are replaced by a broad amorphous scattering feature, indicating that pressure-induced amorphization has occurred (Fig. 2). There is no evidence for the appearance of any high-pressure metallic Si or Rb phases so we conclude that the amorphous material has $Rb_{6.15}Si_{46}$ composition.

X-ray diffraction patterns obtained during decompression are shown in Fig. 4. There is no evidence for recrystallization and an amorphous form of $Rb_{6.15}Si_{46}$ is recovered to approximately ambient pressure. During decompression, the main amorphous diffraction feature shifts approximately linearly to lower 2θ values (i.e., larger d spacing). We could not carry out any more detailed analysis of the amorphous scattering as done in Ref. 44 because of the scattering contribution of the N_2 pressurization medium, the presence of strong Bragg diffraction from the TaN/TaO impurity/standards, and the lack of proper background pattern recorded during the experiment.

The V/V_0 data for $Rb_{6.15}Si_{46}$ upon compression in the low-pressure range 0.1–24 GPa were initially fitted using a third-order Birch-Murnaghan equation of state model to obtain the bulk modulus K_0 and its pressure derivative K_0' for the clathrate phase. The values obtained by this procedure were K_0=59(1) GPa and K_0'=7.2(2), respectively. Frequently, few details of the fitting procedure are given and the

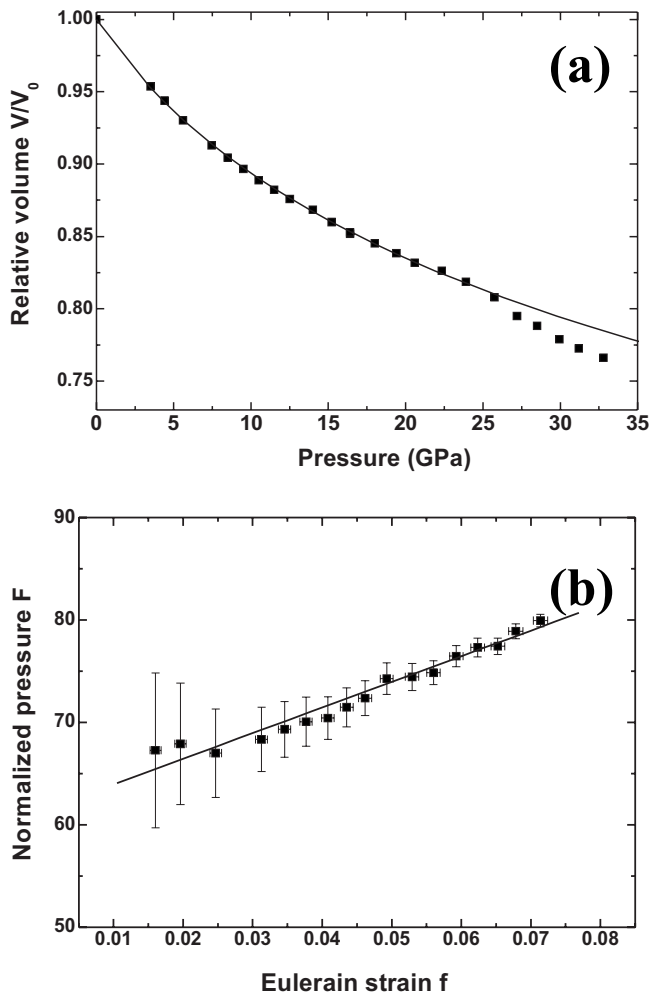

FIG. 3. (a) V/V_0 plot for $Rb_{6.15}Si_{46}$ as a function of pressure (points) along with a third-order Birch-Murnaghan equation of state fitted to the data with K_0=61.4(7) GPa and K_0'=6.7(2) (solid line). The K_0 and K_0' values were obtained from a reduced variable (F-f) plot. (b) Plot of the normalized pressure (F) as a function of the Eulerian strain variable (f) for $Rb_{6.15}Si_{46}$.

value of K_0' assumed or fitted is not quoted. Because $V(P)$ constitutes a nonlinear relation, it is not always easy to design a goodness of fit criterion and to choose the best set of K_0, K_0', and V_0 parameters. The alternative fitting procedure used here involves transformation of the $V(P)$ data to the normalized or reduced stress-strain variables F and f (Fig. 5).[45] The Eulerian strain parameter (f) and the normalized pressure F are defined by

$$f = \frac{1}{2}\left[\left(\frac{V}{V_0}\right)^{-2/3} - 1\right], \tag{1}$$

$$F = P[3f(1+2f)^{2.5}]^{-1}. \tag{2}$$

This formalism yields the second-order finite strain equation

$$F = K_0[1 - 1.5(4 - K_0')f]. \tag{3}$$

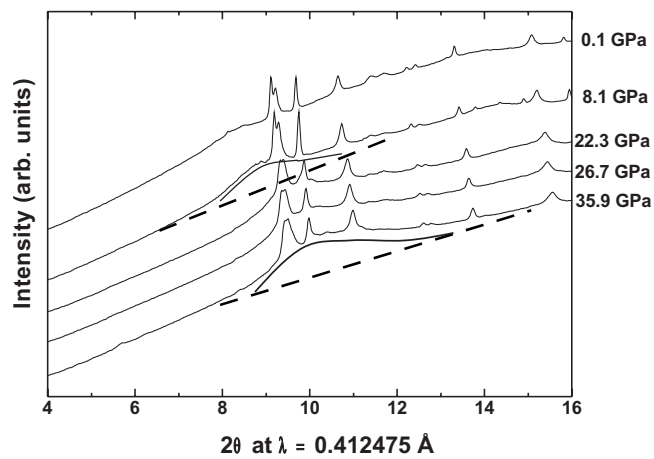

FIG. 4. Selected x-ray diffraction patterns during decompression. The broad feature under the crystalline peaks of TaN and TaO are due to the amorphous Rb-Si alloy obtained at pressure higher than 33 GPa. Dashed lines and solid lines are guides for the eyes, emphasizing the background and the amorphous halo, respectively.

We can then conduct a linear fit to the resulting F-f plot. In that case, well accepted goodness of fit criteria can be applied to the linear fit and likely vs unlikely ranges of values for K_0' can be readily tested against the data within its error bars. K_0 and K_0' were then obtained as the intercept as $f \to 0$ and the slope of the F-f plot, respectively. This procedure yielded final values of K_0=61.4(7) GPa and K_0' =6.7(2) for a measured V_0=1088.4 Å^3.

We also took the opportunity to determine K_0 and K_0' for TaO that has not yet been reported in the literature. Using an F-f plot, the values K_0=293(3) GPa and K_0'=5.4(3) were obtained for a measured V_0 of 88.0(2) Å^3.

The presence of ε-TaN and TaO as internal standards presents within the sample, neither of which undergo any phase transitions throughout the pressure range studied, permitted us to make a more detailed analysis of the x-ray diffraction peak widths and intensities of $Rb_{6.15}Si_{46}$ clathrate during pressurization, as well as discriminating between changes intrinsic to the clathrate structure and possible effects due to the sample environment. The three most intense Bragg peaks of $Rb_{6.15}Si_{46}$ [(222), (320), and (321)] are situated at 2θ values of 7.96°(1), 8.29°(1), and 8.60°(1), respectively, at ambient pressure. The shape of each peak was fitted using a pseudo-Voigt function. In Fig. 5(a) we show the changes in d spacings of these peaks between 0–20 GPa. The slopes can be fitted as two linear regimes with an apparent change of slope at $P \sim 13$ GPa. At first glance, one could argue that this is not surprising as a nonlinear variation of the d spacings with pressure is expected. However, carrying out a reduced variable F-f analysis for the three reveals a possible discontinuity at $P \sim 13$ GPa that is reflected in the behavior of the (320) and (321) reflections [Figs. 5(c) and 5(d)]. That result is corroborated by the Raman-scattering data presented below that reveal a change in the spectra occurring at this pressure. We then compare the width of the clathrate peaks normalized to that of the most intense peak of TaO (Fig. 6). There is an initial broadening of the clathrate peaks with initial pressurization (that cannot be due to any nonhydro-

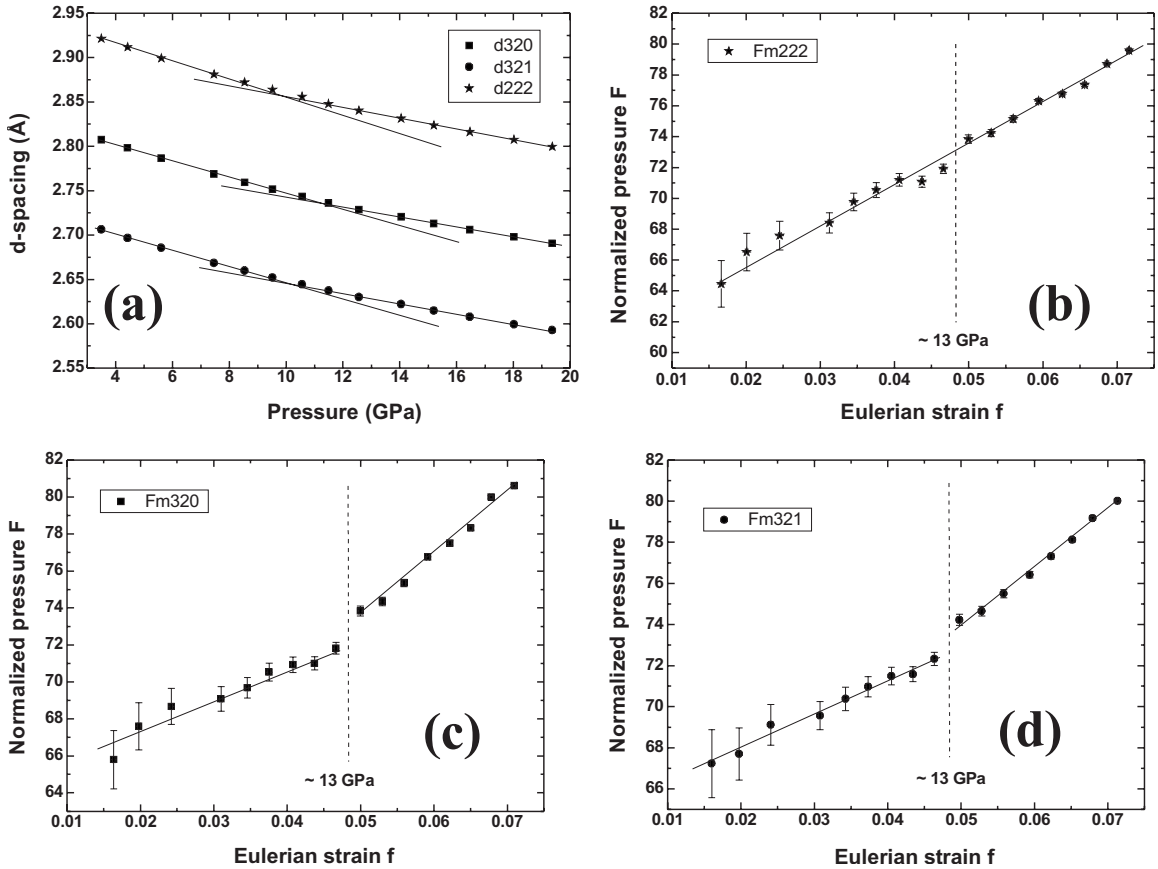

FIG. 5. (a) Change in d spacing for (320), (321), and (222) clathrate reflections with increasing pressure. Two regimes are distinguished with a transition occurring at around 13 GPa. (b) Linearized F-f plot based on the data obtained for the (222) peak. (c) F-f plot from the (320) peak data. (d) F-f from the (321) peak data.

static conditions developing within the sample) up to $P \sim 12$ GPa. Then there is a dramatic increase in the peak width for all three reflections, peaking at $P \sim 13$ GPa, before returning to the width obtained just before the transition. This significant broadening around 12–13 GPa may be due to the coexistence of two phases with very close cell parameters. This coexistence would exist on a narrow pressure range, either because of the first-order character of the transition or due to the pressure gradient in the volume probed by the x-ray beam. Further pressurization results in a slight decrease in peak width for the (222) and (321) reflections, up to the point of amorphization ($P \sim 30$ GPa). It is interesting that the "volume collapse" transition observed in the $V(P)$ plot at $P \sim 24$ GPa is not accompanied by any observable change in the peak widths of the principal clathrate reflections calibrated using this method. Based on the linewidth observations and also the Raman spectroscopy results described below, we suggest that some structural transformation occurs within the $Rb_{6.15}Si_{46}$ clathrate structure at $P \sim 13$ GPa. These detailed changes are not readily visible on the V/V_0 plot (Fig. 4). However, they represent a sudden change to some d_{hkl} values for the clathrate that are not obviously expressed in all of the reflections. We have carried out a detailed examination of the stress-strain relations in the clathrate using F-f relations, first for the three principal reflections then for all 32 peaks used in the global Le Bail refinement, and we can detect a significant change in slope at the transition point (Fig. 5). We have fitted the F-f relations below and above the transition with two linear regions to estimate K_0 and K_0' (Table I). We find that the transition at 13 GPa is associated with a slight (7.5%) decrease in K_0 and a 20% increase in K_0'; i.e., the clathrate structural modification above the transition range is mechanically "softened" in that it is more compressible and its compressibility changes more rapidly with pressure.

At pressures above the volume collapse ($P > 24$ GPa), data were analyzed using a third-order Birch-Murnaghan equation of state. The fitted values obtained are $V_0 = 1241(80)$ Å^3, $K_0 = 48(18)$, and $K_0' = 2.8(5)$.

In conclusion, our angle-dispersive synchrotron x-ray diffraction studies and subsequent analysis of the data indicate that $Rb_{6.15}Si_{46}$ undergoes two phase transformations at $P \sim 13$ GPa and $P = 24 \pm 1$ GPa. Both are apparently isostructural transformations in the sense that no additional reflections or peak splittings are observed to indicate a deviation from the $Pm\bar{3}m$ cubic clathrate structure. However, a slight distortion of the cubic structure cannot be discarded. The different pressure behaviors of the (222), (320), and (321) d spacings observed in Fig. 5 are not expected to occur in a strictly cubic structure. The first "transition" at ~ 13 GPa is associated with a marked broadening in the principal (222), (320), and (321) reflections over a narrow pressure range and it corresponds to an abrupt change in the K_0 and K_0' values of the clathrate crystal. The second transition is associated with

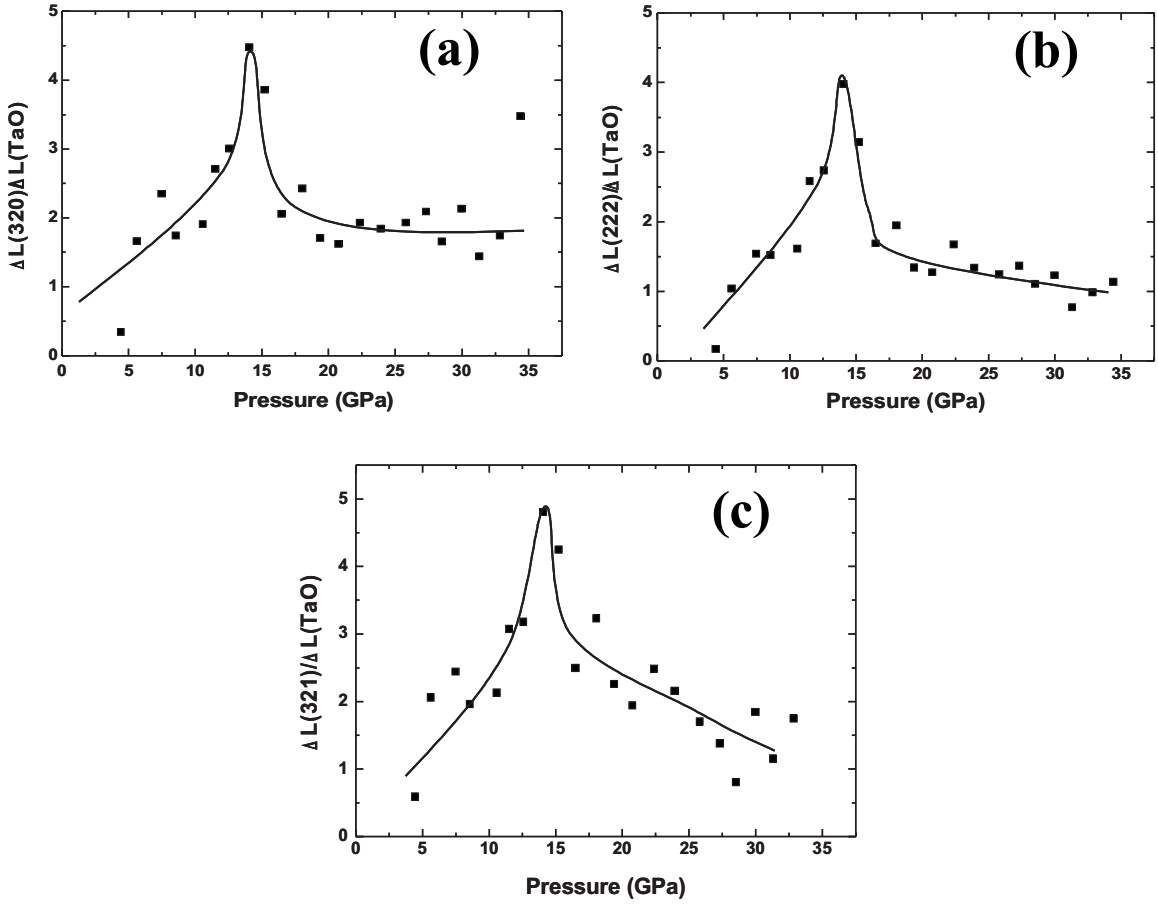

FIG. 6. TaO is used as an internal standard to estimate intrinsic broadening of the clathrate peak. Ratio of the width of selected $Rb_{6.15}Si_{46}$ reflections with respect to the width of the TaO (222) peak: (a) $Rb_{6.15}Si_{46}$ (320), (b) $Rb_{6.15}Si_{46}$ (222), and (c) $Rb_{6.15}Si_{46}$ (321).

an abrupt change to a more negative slope in the $V(P)$ relation and it seems to correspond to the "volume collapse" transition previously described for K_8Si_{46}, Ba_8Si_{46}, and $I_8Si_{44}I_2$ clathrates.[5]

Finally, pressure-induced amorphization (PIA) occurs at 33 ± 1 GPa, when the V/V_o value has attained ~ 0.77 (i.e., $V \sim 838$ Å^3). The sample does not show evidence of crystallization into any of the stable or metastable high-pressure phases of Si (or to produce elemental Rb) at high pressure following PIA or during decompression to ambient conditions (Fig. 3). We could not carry out any quantitative analysis of the amorphous x-ray diffraction patterns, but the main amorphous diffraction feature was observed to shift to lower 2θ values as the pressure was released. We investigated the detailed behavior of the amorphous $Rb_{6.15}Si_{46}$ material produced via PIA during decompression using Raman spectroscopy, described in Sec. III B.

TABLE I. K_0 and K_0' values obtained from a reduced variable (F-f) plot analysis for the (222), (320), and (321) reflections and from the global LeBail refinement of lattice parameters and unit-cell volume. Two regimes were considered: the low-pressure regime up to 13 GPa and the high-pressure regime from 13 to 24 GPa.

	Low pressure (0–13 GPa)		High pressure (13–24 GPa)	
	K_0 (GPa)	K_0' (GPa)	K_0 (GPa)	K_0' (GPa)
(222)	61.4(6)	6.5(6)	60.3(8)	6.9(4)
(320)	63.8(5)	5.8(6)	56.5(9)	8.0(5)
(321)	64.7(3)	5.7(3)	60.0(6)	7.1(3)
Global	64.0(9)	5.7(9)	60(1)	7.0(7)

B. Raman spectroscopy

The expected Raman-active modes for the clathrate type-I structure are predicted using symmetry analysis. 54 atoms located within the primitive unit cell corresponding to space group $Pm\bar{3}n$ (i.e., O_h^3) give rise to 162 zone-center ($\mathbf{k}=0$) vibrational modes. Those that are predicted to be Raman active are

$$\Gamma_{\text{Raman}} = 3A_{1g} + 8E_g + 9T_{2g}.$$

Two Raman-active modes of symmetry E_g and T_{2g} are expected to occur at low frequency (<200 cm^{-1}), mainly involving the encapsulated Rb atoms in the large (6d) guest sites.[46–49] These modes are uncoupled from the framework vibrations and they are thought to play an important role in determining the anomalously low lattice thermal conductivity of the clathrate structures.[50,51] The remaining modes are associated with Si-Si stretching and bending vibrations of the

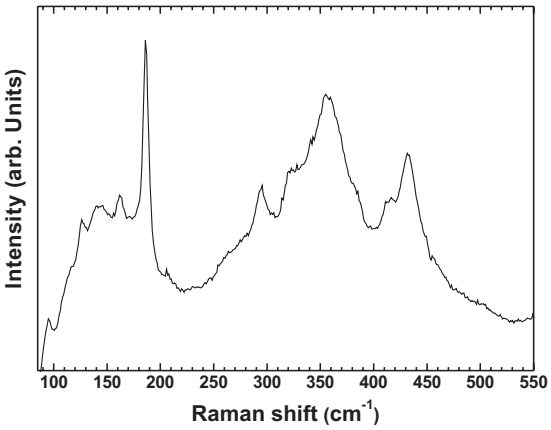

FIG. 7. Raman spectrum of $Rb_{6.15}Si_{46}$ measured at 1 atm and room temperature.

clathrate framework. The Raman spectrum at ambient conditions (Fig. 7) is in good agreement with those previously reported for analogous type-I clathrates (i.e., K_8Si_{46} and Ba_8Si_{46}).[28] Usually, most of Raman bands are broad. In some cases, these broad bands may contain unresolved Raman lines and less Raman bands than expected are observed. In the case of $Rb_{6.15}Si_{46}$, our experimentally accessible spectral range is situated above 120 cm^{-1} and all the observed modes are assumed to be related to the Si framework. Using the calculated frequency by *ab initio* simulations as a starting model for the Lorentzian line-shape analysis, we obtained a good agreement (within 5%) with the calculations (Table II).

The Raman spectrum recorded by Fang *et al.*[47] for the fully filled clathrate Na_8Si_{46} is quite different from the spectrum for $Rb_{6.15}Si_{46}$ at ambient pressure. The sharp low-frequency peaks all occur at lower wave number (<150 cm^{-1}) and the strong massif near 370 cm^{-1} is absent. It is not yet clear why this is the case. The Raman spectrum of Ba_8Si_{46} clathrate obtained at ambient pressure is generally similar to those of K_8Si_{46} and $Rb_{6.15}Si_{46}$, but with most of the modes shifted to lower wave number. The linewidths and relative intensities of the Raman modes observed for the metallic type-I clathrates are obviously affected by electron-phonon coupling and also by the presence of guest site vacancies (or other crystal defects) that may eliminate $k=0$ selection rules.[47] The high-frequency modes due to Si-Si stretching along with some deformation vibrations of the clathrate framework are generally broadened compared to the low-frequency modes that are mainly associated with guest atom vibrations. We do not yet have a precise understanding of the factors governing the line shape, width, and relative Raman intensities of high- vs low-frequency modes in these semiconductor/metallic clathrate compounds and their relationship to order/disorder phenomena among the framework and guest atom sites and details of the electronic structure.

1. Quasihydrostatic compression

During the first series of Raman experiments, argon was used as the pressure-transmitting medium to provide a quasi-hydrostatic compression. Figure 8 shows Raman spectra of

TABLE II. Experimental and calculated zone-center Raman peak positions and their pressure derivative for $Rb_{6.15}Si_{46}$. The experimentally accessible spectral range is situated above 120 cm^{-1}. Some peaks could not be determined under high-pressure conditions.

Mode symmetry	Frequency (calculated)	Frequency (measured)	$(\partial\nu/\partial P)$ (calculated)	$(\partial\nu/\partial P)$ (measured)
T_{2g}	72.5	Not accessible	1.7	Not accessible
E_g	89.6	Not accessible	2.3	Not accessible
T_{2g}	122.7	126.0	0.9	0.3(1)
E_g	138.0	141.3	2.3	0.4(1)
T_{2g}	155.7	164.4	−0.2	−0.9(1)
T_{2g}	178.7	186.3	−1.0	−1.2(1)
E_g	203.9	207.2	3.8	Not determined
E_g	259.1	268.0	6.1	Not determined
T_{2g}	286.4	294.9	5.5	3.1(4)
A_{1g}	314.7	320.7	5.2	3.7(5)
E_g	333.1	337.2	10.0	12(2)
A_{1g}	344.3	353.7	11.7	Not determined
E_g	369.2	361.1	8.5	Not determined
T_{2g}	374.8	371.6	7.3	Not determined
E_g	393.8	384.5	8.3	Not determined
E_g	399.9	398.3	7.5	Not determined
T_{2g}	403.9	413.3	6.6	Not determined
T_{2g}	415.9	431.7	7.3	5.4(2)
A_{1g}	423.6	434.3	7.9	4.7(2)
T_{2g}	438.5	457.7	6.2	Not determined

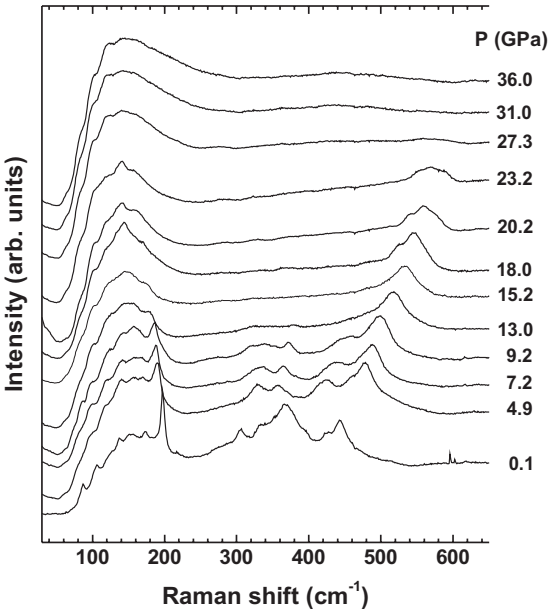

FIG. 8. Raman spectra of $Rb_{6.15}Si_{46}$ during quasihydrostatic compression (using argon as pressure-transmitting medium).

$Rb_{6.15}Si_{46}$ at selected pressures up to 36 GPa and the pressure dependencies of the Raman frequencies are shown in Fig. 9. During the compression experiments, only nine Raman peaks observed at ambient pressure could be significantly followed.

Between ambient pressure and 9.2 GPa, all the high-frequency peaks (>300 cm^{-1}) shift to higher wave number with increasing pressure. However, the most intense Raman mode initially at 186 cm^{-1} shifts to lower frequency, as does the weak shoulder at 164 cm^{-1}, indicating some softening of

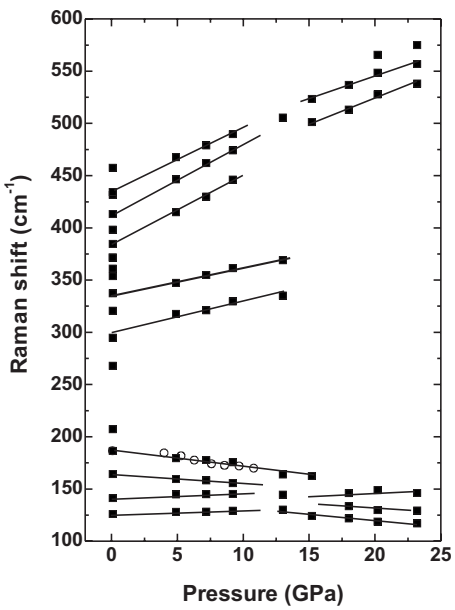

FIG. 9. Raman frequencies of $Rb_{6.15}Si_{46}$ plotted as a function of pressure (for quasihydrostatic compression). Lines are drawn as visual aids. Open symbols: Raman frequency of the most intense peak under nonhydrostatic compression.

these vibrational modes The other low-frequency modes stiffen slightly with pressure, but much less that the high-frequency vibrations. Similar observations were made for Ba_8Si_{46} and K_8Si_{46} type-I clathrates.[28,29] Kume *et al.*[28] noted an analogy with softening in low-lying TA modes at the Brillouin-zone boundary in diamond-structured Si that may be related to the clathrate behavior and could be intrinsic to the sp^3-bonded tetrahedral lattice. Our *ab initio* simulations reproduced this behavior in excellent agreement with the experimental results (Table II).

The appearance of the Raman spectrum is affected significantly by increasing pressure. Important changes in the entire spectrum are observed starting from 9.2 GPa but some of the initial peaks can be followed to 13.0–15.2 GPa but already show a strong attenuation above 9.2 GPa. Examining of the $d\nu/dP$ pressure variation of modes and their appearance and disappearance, it seems that a likely phase transformation occurs near 13 GPa, at the same pressure at which an anomalous broadening in certain x-ray reflections and a mechanical softening of the clathrate lattice are observed. By 18 GPa, an entirely new Raman spectrum is recorded, indicating that a change in the clathrate structural parameters affecting the Raman selection rules has occurred. The soft mode initially at 186 cm^{-1} disappeared and others peaks are replaced by broad bands.

As the pressure is increased, a new peak maximum is identified on the low-frequency shoulder (at $\sim$133 cm^{-1}) that has a negative $d\nu/dP$ dependence (Fig. 9). The high-frequency band ($\sim$505 cm^{-1}) exhibits a new peak at lower wave number for $P>18$ GPa (Fig. 8). These changes in the Si-Si stretching vibrations indicate changes in the clathrate crystal structure and the Raman selection rules occurring in the 18–23 GPa range that are associated with the "volume collapse transition" observed in the $V(P)$ relations derived from the synchrotron x-ray diffraction results.

The crystalline peaks are readily observed in the Raman spectrum up to $P\sim23$ GPa and they can hardly be distinguished at $P=27.3$ GPa (Fig. 8) after the volume collapse according to x-ray diffraction results. Above 31 GPa, the Raman spectrum contains only two very broad and weak bands at $\sim$450 and $\sim$160 cm^{-1} that indicate an amorphous structure. This is correlated with the pressure-induced amorphization event indicated by the x-ray diffraction results (Fig. 2).

The amorphous $Rb_{6.15}Si_{46}$ Raman spectrum obtained at 36.0 GPa using argon as a pressure-transmitting medium (Fig. 8) closely resembles that of the high-density (HDA) metallic amorphous form of elemental Si that has atoms in high (fivefold, sixfold) coordination. In amorphous HDA Si, the spectra consist on a single broad feature between 200 and 700 cm^{-1}, with maximum near 400 cm^{-1}. This is similar to the envelope of bands in the vibrational density of states (VDOS) calculated for crystalline silicon with the β-Sn structure at high pressure and presumably other high-density polymorphs.[52,53] Our results suggest that pressure destabilization of the $Rb_{6.15}Si_{46}$ clathrate, following the volume collapse transition within the clathrate structure, results in formation of a high-density amorphous material with highly coordinated Si atoms that could be structurally related to the HDA form of elemental *a*-Si. During decompression, the

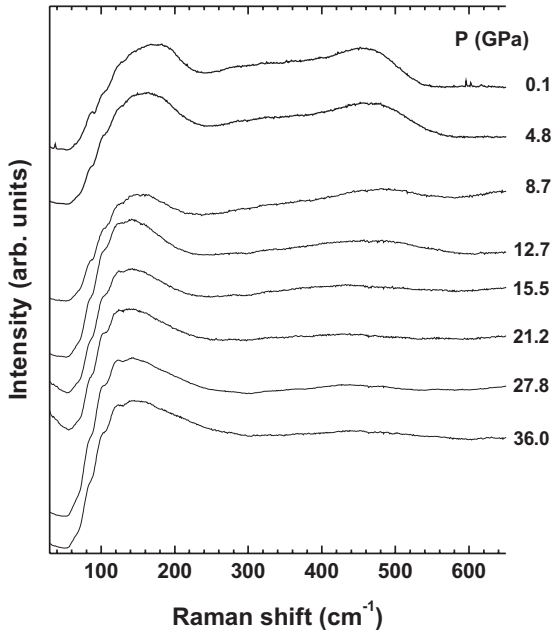

FIG. 10. Raman spectra of $Rb_{6.15}Si_{46}$ during decompression after quasihydrostatic compression to 36 GPa.

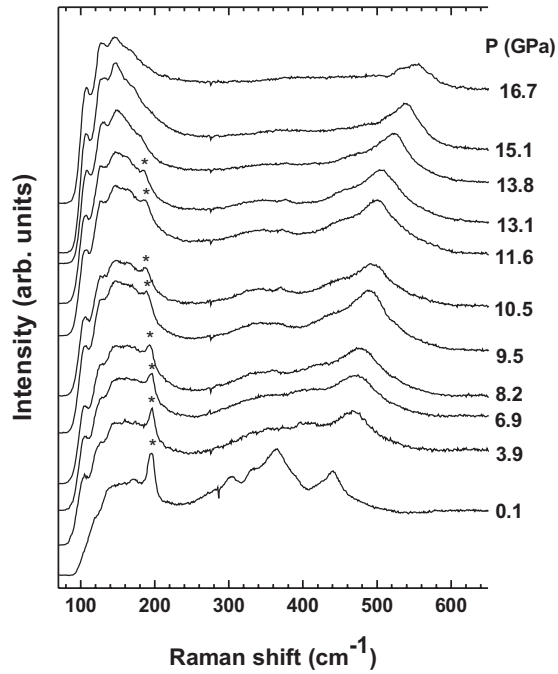

FIG. 11. Raman spectra of $Rb_{6.15}Si_{46}$ during a nonhydrostatic compression (no pressure-transmitting medium) to 16.7 GPa. Asterisk shows the initially most intense peak at around 190 cm^{-1}.

amorphous spectrum changes markedly below 8.7 GPa, with the emergence of a broad feature in the Si-Si stretching region at higher wave number ($\sim$460 cm$-$1) that is more intense than the previous band of the high-density amorphous form (Fig. 10). The spectrum obtained at ambient conditions resembles that of the tetrahedrally coordinated semiconducting low-density amorphous (LDA) polyamorph of *a*-Si dominated by the tetrahedral Si-Si stretching vibration at 450 cm^{-1} and a weaker angle-bending mode at around 300 cm^{-1}. These features reflect a broadened version of the VDOS of the crystalline semiconductor.[53] Our results indicate that the HDA form of $Rb_{6.15}Si_{46}$ produced by PIA from the clathrate has undergone a back transformation into an LDA polyamorphic form during decompression, analogous to the behavior of HDA *a*-Si produced by PIA from nanocrystalline porous-Si or from *a*-Si samples.[52,53]

2. Nonhydrostatic compression

It is known that nonhydrostatic stresses can affect the nature and pressure range of crystalline phase transitions or favor pressure-induced amorphization.[54,55] We submitted $Rb_{6.15}Si_{46}$ to a highly nonhydrostatic stress regime by squeezing it without any pressure-transmitting medium. Figure 11 shows the Raman spectra obtained with increasing pressure up to 16.7 GPa. The Raman results during compression were comparable to those observed during the hydrostatic compression experiment (Figs. 8 and 11). We observed an expected broadening of the Raman modes (particularly between 250 and 450 cm^{-1}). However, the spectrum at 10.5 GPa under nonhydrostatic pressure (Fig. 11) is similar to that obtained at 9.2 GPa during hydrostatic compression (Fig. 8). The pressure dependence of the most intense peak (at 186 cm^{-1} at ambient pressure) is identical in both cases (Fig. 9). A gradual disappearance of the Raman lines characteristic of the low-pressure phase is observed between 11.6 and 15.1 GPa. The spectrum obtained at 16.7 GPa, the highest pressure achieved in that run and that lies lower than the pressure of amorphization, is similar to that obtained during hydrostatic compression at the same pressure. On decompression, we observed a gradual crystal-crystal transformation (Fig. 12). The low-pressure spectra can be interpreted as a superposition of the high-pressure polymorph and the initial low-pressure spectrum, indicating that the crystal structure changes occurring in the 13–18 GPa pressure range could correspond to a first-order phase transition because both phases appear to coexist in the decompressed sample.

IV. DISCUSSION

Our data for the bulk modulus of $Rb_{6.15}Si_{46}$ allow us to further examine the systematics of volume compressibility among Si-framework clathrate-I phases.[5] One of the striking results of our study is that our value of K_0 for Rb_6Si_{46} [61.4(7) GPa] appears to be much smaller than those reported previously for K_8Si_{46} (86 ± 5 GPa), Ba_8Si_{46} (93 ± 5 GPa), $I_8Si_{44}I_2$ (95 ± 5 GPa), or for (94 GPa) or the hypothetical empty cage clathrate Si_{46} (87–88 GPa) studied theoretically.[5,56,57] We must first examine whether the large apparent difference in bulk modulus values recorded for the different clathrates reflect real differences in the elastic behavior or if they are due to the details of the various experiments and fitting procedures used to obtain K_0 from the experimental or theoretical $V(P)$ data. In all of the previous studies, the nonlinear $V(P)$ relation was fit directly using a Murnaghan or Birch-Murnaghan equation of state with K_0' fixed at 3.6. A detailed analysis based on our data rules this

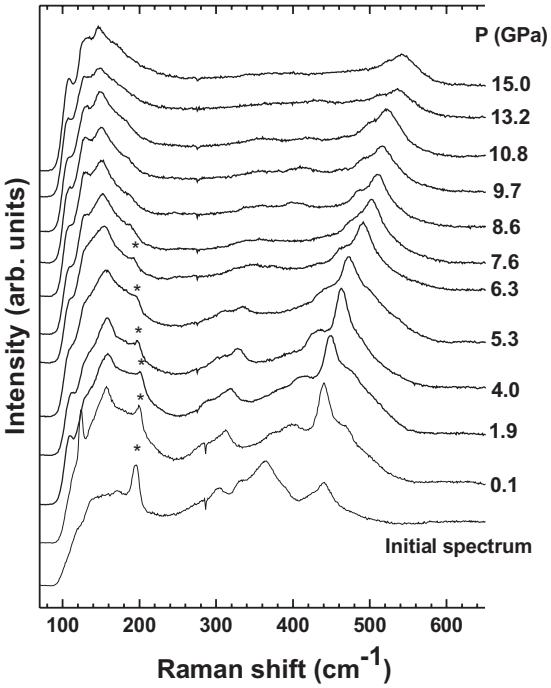

FIG. 12. Raman spectra of $Rb_{6.15}Si_{46}$ during decompression after nonhydrostatic compression to 16.7 GPa. Asterisk shows the initially most intense peak of the clathrate structure at around 190 cm^{-1}.

out as a viable possibility. If we had fixed K_0' at 3.6 in our present study of $Rb_{6.15}Si_{46}$ clathrate, we would have obtained $K_0=78(1)$ GPa, in better apparent agreement with the bulk modulus values reported in previous studies on other type-I clathrates. However, only larger values of K_0' gave a satisfactory fit to our data; this is especially apparent from considering the linearized *F-f* plot (Fig. 5; Table I). Recent neutron-diffraction results obtained on Ba_8Si_{46} compressed with an ethanol-methanol mixture gave $K_0=67(2)$ GPa and $K_0'=8(1)$,[58] in close agreement with our values for $Rb_{6.15}Si_{46}$. *Ab initio* simulations on Ba_8Si_{46} carried out in the present study predict $K_0=77$ GPa and $K_0'=4.2$ (Table III). Thus, it appears that K_0 and K_0' are highly sensitive to the hydrostaticity conditions. Our conclusion is that the compressibility of $Rb_{6.15}Si_{46}$ is larger than Ba_8Si_{46} or other fully filled clathrates, but to a lesser extent than originally thought by an analysis of the data existing in the literature. We used *ab initio* methods to calculate the cell parameter, the bulk modulus K_0, and its derivative K_0' for Ba_xSi_{46} and Rb_xSi_{46} with varying metal cage site occupancies of $x=0$, 2, 6, and 8. The results are summarized in Table III and Fig. 13. Filling the cages with guest atoms increases the cell parameter by up to 1.6% and 1.8% for Ba_8Si_{46} and Rb_8Si_{46}, respectively. The mechanical properties are not strongly affected (less than 2–3 %) by cage occupancy except when the small Si_{20} cages start to be filled with Rb atoms. The filling of all the Si_{20} cages leads to a decrease of K_0 by 10% and an increase of K_0' by 15%. These results clearly show that the presence of Rb atoms in the Si_{20} cages deteriorates the mechanical properties of the clathrate. Therefore, the fact that 24% of the Si_{20} cages are filled with Rb atoms in the sample studied here is cer-

TABLE III. Systematic changes in cell parameter a_0, the bulk modulus (K_0), and its pressure derivative (K_0') with the progressive filling of the nanocages ($x=0$, 2, 6, and 8) in the type-I clathrate structure obtained from *ab initio* calculations.

	a_0	K_0	K_0'
Si_{46}	10.2296	76.055	4.0886
Ba_2Si_{46}	10.2781	77.59	4.0516
Ba_6Si_{46}	10.3092	77.59	4.4531
Ba_8Si_{46}	10.395	76.813	4.2288
Rb_2Si_{46}	10.28	76.185	3.9799
Rb_6Si_{46}	10.3335	74.554	4.1928
Rb_8Si_{46}	10.4148	69.341	4.6828

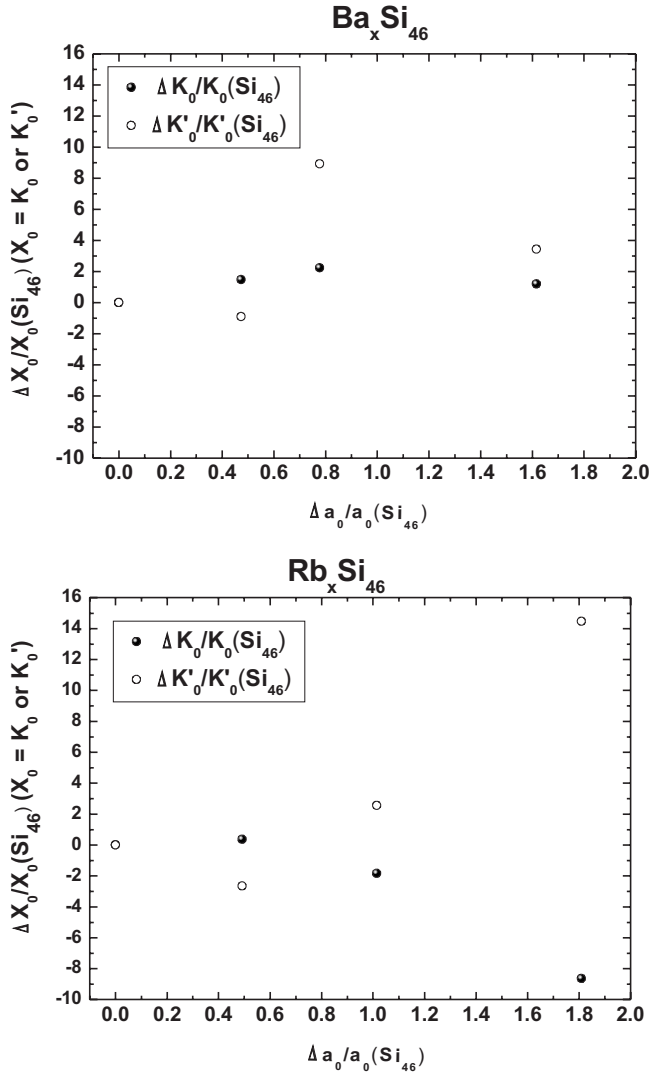

FIG. 13. *Ab initio* calculated systematic changes in the bulk modulus (K_0) and its pressure derivative (K_0') as a function of the cell parameter a_0 with progressive filling of the nanocages ($x=0$, 2, 6, and 8) in the type-I clathrate structure. In Ba_xSi_{46}, the effect on K_0 and K_0' is negligible. In Rb_xSi_{46}, as soon as the smaller Si_{20} cages begin to be filled the structure begins to become mechanically weaker.

tainly the reason why the bulk modulus is slightly lower than the values recorded for other type-I clathrates.

The analysis of individual peaks in the x-ray diffraction patterns and Raman spectra indicate a phase transition occurring at around 13 GPa. As it is shown in Fig. 2, in phase 1 (between ambient P and ~ 12 GPa), a progressive reduction of the intensity of these peaks is observed (Fig. 2 inset). These changes could be interpreted as a progressive introduction of disorder into the structure. Disorder due to guest atom displacement with respect to the center of the nanocages has in fact been observed to accompany Na intercalation in clathrates at room pressure.[59] Nevertheless, it has been shown that such off-center guest displacement is not compatible with large guest atoms such as Rb.[60] Disordering associated with compression of phase 1 should then involve the Si framework. Such distortion of the nanocage framework would be compatible with a loose on the cohesive energy and hence with a lowered value of K_0 observed at the transition

Raman spectroscopy is a local probe with a short coherence length and is more sensitive to static disorder than x-ray diffraction as illustrated in relaxor materials for instance.[61] At pressure above 13 GPa, the Raman spectra show only broad features. This suggests that a disordered displacement of Si atoms without change of their average position (accounted by x-ray diffraction) induces a relaxation of the Raman selection rules. The nature of this transition and the induced distortion requires more studies to understand its role on the volume collapse.

Our data on the $V(P)$ relations in $Rb_{6.15}Si_{46}$ clathrate show that a homothetic "volume collapse" transition occurs at 24 GPa, analogous to those previously observed for the type-I clathrates Ba_8Si_{46}, K_8Si_{46}, and $I_6Si_{44}I_2$, but not for Na_8Si_{46}.[5,27–31] These anomalies in the $V(P)$ relations most likely correspond to an unusual type of symmetry-conserving phase transition.[5] Various explanations for the transition have been proposed, including the presence of electronic[30,62] or phonon instabilities,[28] or possibly vacancy formation on the framework silicon sublattice.[63] X-ray absorption studies on Ba_8Si_{46} show a discontinuity in the Ba K-edge position that could indicate a change in electronic structure at the transition.[30] Tse *et al.*[27] suggested an interpretation in which entire phonon branches associated with K guest atom displacements become unstable in K_8Si_{46} at the transition pressure, resulting in positionally disordered form of the clathrate. Itaka has recently proposed a model in which vacancies could occur on silicon framework sites to yield a defective clathrate Ba_8Si_{43}, analogous to the family of isomorphous E_8Ge_{43} (E: electropositive element) materials in which where there are always Ge vacancies.[63] However, recent accurate x-ray measurements performed on Ba_8Si_{46} in highly hydrostatic conditions did not detect the formation of any amorphous or crystalline high-pressure Si phases after the collapse.[64] Other recent results using a combined Rietveld and maximum-entropy approach to analyze the x-ray diffraction data suggest that the volume collapse transition of Ba_8Si_{46} could be associated with s-p-d rehybridization of the Si atoms at high pressure, leading to a weakening of the Si-Si bonds and a collapse of the unit-cell volume without changing the crystalline structure.[62] In this interpretation of Tse *et al.*[62] (and also proposed by San Miguel *et al.*[30]), the volume collapse can be traced to an electronic topological transition involving a substantial rearrangement of the valence electron distribution accompanied by positional disordering in the Si sites. The Si-Si bonding electrons are removed from the bonding region leading to the weakening of the Si-Si bonds, resulting in a displacive but isostructural phase transition taking place with a large volume reduction. The pressure at which the volume collapse occurs should be controlled by the valence number of the cation. K_8Si_{46} and $Rb_{6.15}Si_{46}$ clathrates containing alkali guest atoms exhibit the volume collapse transition at 23 ± 3 and 24 ± 1 GPa, respectively, whereas Ba_8Si_{46} collapses at a significantly lower pressure 13 ± 2 GPa.[5]

It has been also proposed that the collapse transition occurs when the unit-cell volume attains a critical value.[26] It occurs for K_8Si_{46} and Ba_8Si_{46} clathrates when the unit-cell volume attains 920–930 Å^3.[5,28] However, in the case of $Rb_{6.15}Si_{46}$, the sharp drop in $V(P)$ is only observed when the unit-cell volume is 885–895 Å^3. However, it is worth noting that the $Rb_{6.15}Si_{46}$ unit-cell volume reaches 920–930 Å^3 in the pressure range 10–15 GPa where a structural instability is observed associated with elastic softening and changes in the Raman spectra. Analogous elastic softening events and potential evidence for a low-pressure structural transformation has also been recorded for K_8Si_{46} and Ba_8Si_{46} at $P = 6-7$ GPa, when the volume attains 1010–1035 Å^3.[5] For $Rb_{6.15}Si_{46}$, the lower pressure isostructural transformation might also have the character of a first-order thermodynamic transition because it appears to be associated with a large hysteresis, as indicated by the Raman-scattering data (Fig. 11).

Complete amorphization is observed by x-ray diffraction at higher pressure (33 GPa). The amorphization pressure occurs in a similar pressure range to that recorded for K_8Si_{46} and Ba_8Si_{46} (40 ± 3 and 32 ± 3 GPa, respectively).

As in previous studies of various framework and other materials, the PIA event can be interpreted as resulting from a frustrated first-order transformation of the system or due to an elastic instability.[27] An important additional question arises in the case of the M_xSi_{46} clathrates, in that they can also exhibit compositional disproportionation into a high-pressure dense form of Si and the alkali or alkaline-earth metal element. This may be the case for Na_8Si_{46} clathrate,[26] but instead K_8Si_{46}, Ba_8Si_{46}, and $Rb_{6.15}Si_{46}$ appear to undergo PIA while maintaining constant chemical composition. The result is an amorphous alkali or alkaline-earth–silicon alloy.

The Raman data for $Rb_{6.15}Si_{46}$ indicate that the amorphous material produced is in a high-density form, similar to the HDA metallic polyamorph of a-Si produced via PIA from nanocrystalline porous-Si or by compressing the low-pressure (LDA) amorphous semiconductor.[44,52,53] It is worth noting that the predominance of pentagonal rings in the clathrate structure leads some authors to use clathrates as crystalline prototypes of amorphous silicon or germanium.[65] Recent works combining high-quality x-ray synchrotron sources and molecular dynamics have been used to investigate high-pressure amorphous structures.[53,66] In addition, pressure-induced amorphization is commonly observed in cagelike crystals. Greaves *et al.*[67–69] described a relationship

between temperature- and pressure-induced amorphization in zeolites accompanied by high-low-density polyamorphic transitions in the resulting amorphous phases. To the best of our knowledge, only little is known about temperature phase diagram of type-I clathrates. These compounds, similar to zeolites, may be expressing similar behavior and further experiments are needed. The observed transformation of high-density amorphous $Rb_{6.15}Si_{46}$ to a low-density polyamorph during decompression indicates that the HDA-LDA transition observed for elemental *a*-Si extends into the binary Si-Rb alloy system and presumably into other semiconductor-metal alloy as, for example, in the Zintl phase $BaSi_2$ where pressure-induced amorphization has been observed to occur at around 13 GPa.[70] This observation provides a useful link between studies of PIA and polyamorphism within various compound metalloid systems such as Al-Ge, Ga-Sb, etc.[71]

V. CONCLUSION

The type-I clathrate $Rb_{6.15}Si_{46}$ at high pressure has been studied by angle-dispersive synchrotron x-ray diffraction, Raman spectroscopy, and *ab initio* calculations. A phase transition has been observed around 13 ± 1 GPa from rapid changes occurring in the Raman spectrum and x-ray linewidths, as well as the bulk modulus. A second volume-contracting phase transition occurs around 24 ± 1 GPa, shown by a sudden change in the $V(P)$ relation. This transition may be associated with an electronic topological transition or a phonon instability, resulting in positional disordering of the framework Si atoms. Pressure-induced amorphization occurs at 33 ± 1 GPa. On decompression, the Raman spectra show changes similar to those observed during the high-density to low-density amorphous transformation in elemental amorphous Si. That result suggests that the HDA-LDA polyamorphic transition extends into the Si-Rb system, and the behavior may be general among amorphous semiconductor-metal alloys that do not undergo compositional phase separation.

In summary, the type-I clathrates have a deceptively simple primitive cubic structure that can exhibit a range of unexpected and as yet unexplained transformations during compression, that involve abrupt changes in the cell volume, elastic parameters and vibrational or electronic spectra while maintaining the same average unit-cell symmetry. These changes could arise due to phonon or electronic instabilities involving the host and guest atom sublattices. It is important to study these transitions, because they provide valuable insights into the behavior of these endohedrally doped fully-condensed "fullerane" structures, and they may provide tuning parameters for developing important electronic and thermoelectric or magnetic properties.

ACKNOWLEDGMENTS

This study was supported by EPSRC-GB under Grant No. EP/D07357X (P.F.M). A.M. and P.R.-H. acknowledge the financial support of the MCYT of Spain under Grants No. MAT2007-65990-C03-03 and No. CSD2007-00045. Part of this research conducted at Oak Ridge National Laboratory's Center for Nanophase Materials Sciences was sponsored by the Scientific User Facilities Division, Office of Basic Energy Sciences, U.S. Department of Energy.

*Present address.

[1] C. Cros, M. Pouchard, and P. Hagenmuller, C. R. Hebd. Seances Acad. Sci. **260**, 4764 (1965).
[2] J. S. Kasper, P. Hagenmuller, M. Pouchard, and C. Cros, Science **150**, 1713 (1965).
[3] C. Cros, M. Pouchard, P. Hagenmuller, and J. S. Kasper, Bull. Soc. Chim. Fr. **7**, 2737 (1965).
[4] J. Gallmeier, H. Schäfer, and A. Weiss, Z. Naturforsch. B **24b**, 665 (1969).
[5] A. San Miguel and P. Toulemonde, High Press. Res. **25**, 159 (2005).
[6] S. Bobev and S. C. Sevov, J. Solid State Chem. **92**, 153 (2000).
[7] N. Jaussaud, P. Toulemonde, M. Pouchard, A. San Miguel, P. Gravereau, S. Pechev, G. Goglio, and C. Cros, Solid State Sci. **6**, 401 (2004).
[8] G. B. Adams, M. O'Keeffe, A. A. Demkov, O. F. Sankey, and Y.-M. Huang, Phys. Rev. B **49**, 8048 (1994).
[9] J. Gryko, P. F. McMillan, R. F. Marzke, G. K. Ramachandran, D. Patton, S. K. Deb, and O. F. Sankey, Phys. Rev. B **62**, R7707 (2000).
[10] X. Blase, P. Gillet, A. San Miguel, and P. Mélinon, Phys. Rev. Lett. **92**, 215505 (2004).
[11] D. Kahn and J. P. Lu, Phys. Rev. B **56**, 13898 (1997).
[12] V. Timoshevskii, D. Connétable, and X. Blase, Appl. Phys. Lett. **80**, 1385 (2002).
[13] H. Kawaji, H. O. Horie, S. Yamanaka, and M. Ishikawa, Phys. Rev. Lett. **74**, 1427 (1995).
[14] S. Yamanaka, E. Enishi, H. Fukuoka, and M. Yasukawa, Inorg. Chem. **39**, 56 (2000).
[15] P. Toulemonde, Ch. Adessi, X. Blase, A. San Miguel, and J. L. Tholence, Phys. Rev. B **71**, 094504 (2005).
[16] E. D. Sloan, Nature (London) **426**, 353 (2003).
[17] Ya. Mudryk, P. Rogl, C. Paul, S. Berger, E. Bauer, G. Hilscher, C. Godart, and H. Noël, J. Phys.: Condens. Matter **14**, 7991 (2002).
[18] G. Ramachandran, P. F. McMillan, J. J. Dong, and O. F. Sankey, J. Solid State Chem. **154**, 626 (2000).
[19] L.-G. Liu and W. A. Bassett, *Elements, Oxides, Silicates: High-Pressure Phases with Implications for the Earth's Interior* (Oxford University Press, New York, 1986).
[20] G. A. Voronin, C. Pantea, T. W. Zerda, L. Wang, and Y. Zhao, Phys. Rev. B **68**, 020102(R) (2003).
[21] S. J. Duclos, Y. K. Vohra, and A. L. Ruoff, Phys. Rev. B **41**, 12021 (1990).
[22] A. Ammar, C. Cros, M. Pouchard, N. Jaussaud, J. M. Bassat, G. Villeneuve, M. Dutine, M. Menetrier, and E. Reny, Solid State Sci. **6**, 393 (2004).
[23] A. San-Miguel, P. Keghelian, X. Blase, P. Melinon, A. Perez, J.

P. Itie, A. Polian, E. Reny, C. Cros, and M. Pouchard, Phys. Rev. Lett. **83**, 5290 (1999).
[24] G. K. Ramachandran, P. F. McMillan, S. K. Deb, M. Somayazulu, J. Gryko, J. Dong, and O. F. Sankey, J. Phys.: Condens. Matter **12**, 4013 (2000).
[25] P. F. McMillan, O. Shebanova, D. Daisenberger, R. Quesada Cabrera, E. Bailey, A. Hector, V. Lees, D. Machon, A. Sella, and M. Wilson, Phase Transitions **80**, 1003 (2007).
[26] A. San Miguel, P. Melinon, D. Connetable, X. Blase, F. Tournus, E. Reny, S. Yamanaka, and J. P. Itie, Phys. Rev. B **65**, 054109 (2002).
[27] J. S. Tse, S. Desgreniers, Z. Q. Li, M. R. Ferguson, and Y. Kawazoe, Phys. Rev. Lett. **89**, 195507 (2002).
[28] T. Kume, T. Koda, S. Sasaki, H. Shimizu, and J. S. Tse, Phys. Rev. B **70**, 052101 (2004).
[29] T. Kume, H. Fukuoka, T. Koda, S. Sasaki, H. Shimizu, and S. Yamanaka, Phys. Rev. Lett. **90**, 155503 (2003).
[30] A. San Miguel, A. Merlen, P. Toulemonde, T. Kume, S. LeFloch, A. Aouizerat, S. Pascarelli, G. Aquilanti, O. Mathon, T. LeBihan, J. P. Itié, and S. Yamanaka, Europhys. Lett. **69**, 556 (2005).
[31] H. Shimizu, T. Kume, T. Kuroda, S. Sasaki, H. Fukuoka, and S. Yamanaka, Phys. Rev. B **68**, 212102 (2003).
[32] H.-K. Mao, J. Xu, and P. M. Bell, J. Geophys. Res. **91**, 4673 (1986).
[33] A. P. Hammersley, S. O. Svensson, M. Hanfland, A. N. Fitch, and D. Hausermann, High Press. Res. **14**, 235 (1996).
[34] E. Soignard and P. F. McMillan, Chem. Mater. **16**, 3533 (2004).
[35] P. Hohenberg and W. Kohn, Phys. Rev. **136**, B864 (1964); W. Kohn and L. J. Sham, Phys. Rev. **140**, A1133 (1965).
[36] G. Kresse, Computer code VASP. See http://cms.mpi.univie.ac.at/vasp
[37] J. P. Perdew, K. Burke, and M. Ernzerhof, Phys. Rev. Lett. **78**, 1396 (1997).
[38] P. E. Blöchl, Phys. Rev. B **50**, 17953 (1994); G. Kresse and D. Joubert, *ibid.* **59**, 1758 (1999).
[39] H. J. Monkhorst and J. D. Pack, Phys. Rev. B **13**, 5188 (1976).
[40] A. Mujica, A. Rubio, A. Muñoz, and R. J. Needs, Rev. Mod. Phys. **75**, 863 (2003).
[41] K. Parlinski, Computer code PHONON. See http://wolf.ifj.edu.pl/phonon
[42] E. Soignard, O. Shebanova, and P. F. McMillan, Phys. Rev. B **75**, 014104 (2007).
[43] J. Rodriguez-Carjaval, Physica B **192**, 55 (1993).
[44] D. Daisenberger, M. Wilson, P. F. McMillan, R. Quesada Cabrera, M. C. Wilding, and D. Machon, Phys. Rev. B **75**, 224118 (2007).
[45] R. J. Angel, in *High-Pressure, High-Temperature Crystal Chemistry*, edited by R. M. Hazen and R. T. Downs, Reviews in Mineralogy and Geochemistry (Mineralogical Society of America and the Geochemical Society, Washington, D.C., 2000), Vol. 41, p. 35–60.
[46] E. Reny, A. San-Miguel, Y. Guyot, B. Masenelli, P. Melinon, L. Saviot, S. Yamanaka, B. Champagnon, C. Cros, M. Pouchard, M. Borowski, and A. J. Dianoux, Phys. Rev. B **66**, 014532 (2002).
[47] S. L. Fang, L. Grigorian, P. C. Eklund, G. Dresselhaus, M. S. Dresselhaus, H. Kawaji, and S. Yamanaka, Phys. Rev. B **57**, 7686 (1998).
[48] G. S. Nolas, C. A. Kendziora, J. Gryko, C. W. Myles, A. Poddar, and O. F. Sankey, J. Appl. Phys. **92**, 7225 (2002).
[49] J. S. Tse, T. Iitaka, T. Kume, H. Shimizu, K. Parlinski, H. Fukuoka, and S. Yamanaka, Phys. Rev. B **72**, 155441 (2005).
[50] J. Dong, O. F. Sankey, and C. W. Myles, Phys. Rev. Lett. **86**, 2361 (2001).
[51] G. S. Nolas, T. J. R. Weakley, J. L. Cohn, and R. Sharma, Phys. Rev. B **61**, 3845 (2000).
[52] S. K. Deb, M. Wilding, M. Somayazulu, and P. F. McMillan, Nature (London) **414**, 528 (2001).
[53] P. F. McMillan, M. Wilson, D. Daisenberger, and D. Machon, Nature Mater. **4**, 680 (2005).
[54] P. Gillet, J. Badro, B. Varrel, and P. F. McMillan, Phys. Rev. B **51**, 11262 (1995).
[55] D. Machon, V. P. Dmitriev, P. Bouvier, P. N. Timonin, V. B. Shirokov, and H.-P. Weber, Phys. Rev. B **68**, 144104 (2003).
[56] C. A. Perottoni and J. A. H. da Jornada, J. Phys.: Condens. Matter **13**, 5981 (2001).
[57] D. Connétable, V. Timoshevskii, E. Artacho, and X. Blase, Phys. Rev. Lett. **87**, 206405 (2001).
[58] P. Toulemonde, D. Machon, M. Tucker and A. San Miguel (unpublished).
[59] F. Brunet, P. Mélinon, A. San Miguel, P. Kéghélian, A. Perez, A. M. Flank, E. Reny, C. Cros, and M. Pouchard, Phys. Rev. B **61**, 16550 (2000).
[60] H. Libotte, J.-P. Gaspard, A. San Miguel, and P. Mélinon, Europhys. Lett. **64**, 757 (2003).
[61] J. Kreisel and P. Bouvier, J. Raman Spectrosc. **34**, 524 (2003).
[62] J. S. Tse, R. Flacau, S. Desgreniers, T. Iitaka, and J. Z. Jiang, Phys. Rev. B **76**, 174109 (2007).
[63] T. Iitaka, Phys. Rev. B **75**, 012106 (2007).
[64] L. Yang, Y. M. Ma, T. Iitaka, J. S. Tse, K. Stahl, Y. Ohishi, Y. Wang, R. W. Zhang, J. F. Liu, H.-K. Mao, and J. Z. Jiang, Phys. Rev. B **74**, 245209 (2006).
[65] F. C. Weinstein and E. A. Davis, J. Non-Cryst. Solids **13**, 153 (1973).
[66] P. F. McMillan, M. Wilson, M. C. Wilding, D. Daisenberger, M. Mezouar, and G. N. Greaves, J. Phys.: Condens. Matter **19**, 415101 (2007).
[67] G. N. Greaves and F. Meneau, J. Phys.: Condens. Matter **16**, S3459 (2004).
[68] G. N. Greaves, F. Meneau, O. Marjérus, D. G. Jones, and J. Taylor, Science **308**, 1299 (2005).
[69] G. N. Greaves, F. Meneau, A. Sapelkin, L. M. Colyer, I. ap Gwynn, S. Wade, and G. Sankar, Nature Mater. **2**, 622 (2003).
[70] T. Nishii, T. Mizuno, Y. Mori, K. Takarabe, M. Imai, and S. Kohara, Phys. Status Solidi B **244**, 270 (2007).
[71] E. G. Ponyatovsky and O. I. Barkalov, Mater. Sci. Rep. **8**, 147 (1992).